remote sensing

MDPI

Article

Range Sidelobe Iterative Suppression Algorithm for Extended Target with Non-Grid Multiple Scattering Points

Jing Xu [1], Yanan Zhang [1], Jindong Zhang [1,*] and Jiarui Chen [2]

[1] The School of Electronic and Information Engineering, Nanjing University of Aeronautics and Astronautics, Nanjing 210000, China; xujing000223@nuaa.edu.cn (J.X.); ya_nanzhang@163.com (Y.Z.)
[2] The 723 Institute of CSSC, Zhenjiang 212000, China; chenjr_nuaa@163.com
* Correspondence: zjdjs@126.com; Tel.: +86-189-1390-3918

Abstract: This paper concentrates on extended targets to suppress high sidelobes in non-grid multiple scattering points. Notice that the problem essentially resolves the high sidelobes of the non-grid multiple scatterers after locating positions; we proposed a novel iterative algorithm based on an adaptive pulse compression algorithm on the basis of an off-grid position estimation. First, the grid offsets of the multiple scattering points through decoherence and super-resolution techniques are estimated by employing an enhanced MUSIC algorithm. Then, an optimization model is constructed for the non-grid multiple scattering points of the target. Finally, a sidelobe suppression algorithm based on the minimum mean square error (MMSE) criterion is presented. Numerical results reveal that the proposed algorithm can achieve better estimation performance on the offsets of the non-grid multiple scattering points, while it suppresses range sidelobes effectively.

Keywords: non-grid multiple scattering points; range sidelobe; improved MUSIC algorithm; iterative suppression; minimum mean square error

Citation: Xu, J.; Zhang, Y.; Zhang, J.; Chen, J. Range Sidelobe Iterative Suppression Algorithm for Extended Target with Non-Grid Multiple Scattering Points. *Remote Sens.* **2023**, *15*, 4811. https://doi.org/10.3390/rs15194811

Academic Editors: Xiaolong Li, Shisheng Guo, Chenguang Shi, Avik Santra and Junkun Yan

Received: 26 June 2023
Revised: 17 September 2023
Accepted: 27 September 2023
Published: 3 October 2023

1. Introduction

Matched filter (MF) is widely applied in pulse compression to solve the contradiction between target detection performance and high-range resolution. However, MF can produce high-range sidelobes. Since a weak target is easily covered by the sidelobes of a strong target, it results in the degradation of target detection performance [1]. Therefore, extensive research has been focused on the sidelobe suppression algorithm in recent years.

It is common to employ the windowing method in sidelobe suppression. However, the windowing algorithm brings about the broadening width of the main lobe and the loss of signal-to-noise ratio (SNR) [2–4]. Mismatch filter (MMF) can also improve the detection ability of weak targets and the ratio of main lobe and sidelobe, but MMF will also increase the main lobe width and introduce SNR loss [5–7]. The CLEAN algorithm proposed in [8] needs to search the locations of the strong targets and then eliminate the influence of the range sidelobes. It can suppress the range sidelobes of the strong targets, while the extraction effect of weak targets is not satisfactory. The least square (LS) method proposed in [9] can acquire better sidelobe suppression performance. However, the processing of scattering points outside the window causes a serious impact on the processing of targets in the window [10,11].

In [12], an adaptive pulse compression (APC) algorithm, which takes the matched filter output as prior information, is proposed by Shannon D. Blunt and Karl Gerlach according to the minimum mean square error (MMSE) criterion. In the APC algorithm, adaptive filters are iteratively calculated with the power value of the adjacent range unit and can effectively suppress range sidelobes. In [13,14], the authors compare the APC algorithm with the mismatched filter and LS method, and prove that the APC algorithm has remarkable sidelobes suppression effect. In addition, considering the Doppler mismatch existing in the target echo, Blunt proposed an APC method based on Doppler

compensation to avoid the performance degradation due to Doppler mismatch [15].The adaptive pulse compression repair (PCR) method is proposed in [16], and it performs APC on the result of MF and has stronger robustness against Doppler mismatch and systematic errors. In order to further reduce the calculation amount of the APC algorithm, Blunt combined a dimension reduction algorithm and proposed the fast adaptive pulse compression (FAPC) method, which includes DFAPC and CFAPC [17,18]. FAPC preserves most performance advantages of APC while reducing the computational effort, but reduces the degrees of freedom of the algorithm and can suppress weak targets in dense targets' environments.

The above APC algorithms assume that the targets are located on the sampling points. Since the targets are randomly distributed with different ranges, the targets will not strictly fall on the sampling points, resulting in sampling mismatch. In APC processing, when targets are not located at the sampling points, the APC result will have great performance loss. In [19,20], Henke proposed to oversample the echo signal to suppress the influence of distance sampling mismatch, but this approach will lead to an increase in computing costs. In [21–23], an APC algorithm based on linear constraint minimum variance (LCMV) criterion is proposed to solve the distance sampling mismatch problem by setting the main lobe's width and interference zero-point's constraint conditions. However, it is difficult to classify relative values of strong and weak targets and conduct quantitative operations.

Based on the above analysis, an iterative suppression algorithm for range sidelobe of the targets with non-grid multiple scattering points is considered in this paper. In our method, an improved MUSIC algorithm is used to estimate the location of multiple scattering points by decoherence and super-resolution [24–27], and an MMSE filter for multiple scattering points is derived to realize the suppression of high sidelobe. The innovation lies in that the MUSIC algorithm originally used for angle measurement can estimate the accurate position of the non-grid targets by constructing the subdivided steering vector after adding a step of dechirp [28–30]. On the basis of obtaining the accurate position, the original grid APC algorithm is improved to the non-grid APC algorithm, which can restrain the high-distance sidelobe. In this way, it avoids covering the small targets and completes the demand of sidelobe suppression. Numerical results verify the effectiveness of the proposed algorithm. The simulation parameters are set to refer to the parameters of the actual maritime detection radar. Parameters of some maritime detection radars are tested data. These echo signals have dense targets and wide sidelobes, and the strong target covers the weak targets, so the algorithm can completely realize the function of detecting the signal.

The structure of this paper is organized as follows. In Section 2, the echo signal model of the target with non-grid multiple scattering points is constructed. Section 3 introduces the range sidelobe iterative suppression algorithm based on the non-grid multiple scattering points model, including the improved MUSIC algorithm and the target sidelobe iterative suppression algorithm based on the non-grid scattering points model. Section 3 also conducts an analysis and comparison of the complexity of the range dimension sidelobe suppression algorithms based on grid targets' echo signals and non-grid targets' echo signals. In Section 4, the proposed algorithm is verified by the simulated and practical measured data, and the algorithm results are provided and analyzed. Section 5 provides conclusions.

2. Model

Target Echo Signal Model of Non-Grid Multiple Scattering Points

The non-grid multiple scattering points model established in this chapter is shown below. The echo signal with unknown targets is constructed by a main scattering point and multiple weak scattering points. Simultaneously, the scattering points are positioned

on the non-grid range points. In this model, the strong point sidelobe will mask the weak point signal.

Let the radar transmit pulse be $s_0(t)$ and it can be rewritten as follows:

$$s_0(t) = \mathrm{rect}\left(\frac{t}{T_\mathrm{p}}\right)\exp\left(\mathrm{j}\pi K t^2\right) \tag{1}$$

where K is the frequency modulation slope, T_p is the pulse width, $\mathrm{rect}(t) = \begin{cases} 1, & |t| \le \frac{1}{2} \\ 0, & \text{else} \end{cases}$.

The echo signal $y(t)$ of the multiple scattering points can be expressed as follows:

$$\begin{aligned} y(t) &= \sum_{q=0}^{Q-1} \alpha_q \mathrm{rect}\left(\frac{t-\tau_q}{T_\mathrm{p}}\right)\exp\left[\mathrm{j}\pi K\left(t-\tau_q\right)^2\right] + n(t) \\ &= \sum_{q=0}^{Q-1} \alpha_q s_0\left(t-\tau_q\right) + n(t) \end{aligned} \tag{2}$$

where the number of strong and weak scattering points is set as Q, in which there are Q_1 non-grid and Q_2 on-grid scattering points, τ_0 is the time delay of the strongest point, $\tau_q\ (q = 0,1,\ldots,Q-1)$ is the time delay of the rest points, $n(t)$ is the additive white noise.

In radar signal processing process, the echo signal $y(t)$ is processed by MF, which takes the convolution of the echo signal with complex conjugation of the transmitted signal. The pulse compression filter output $y_\mathrm{MF}(t)$ is as follows:

$$\begin{aligned} y_\mathrm{MF}(t) &= y(t) * s_0^*(t) \\ &= \sum_{l=0}^{Q-1} \sqrt{BT_\mathrm{p}}\,\frac{\sin\left[\pi B\left(t-\tau_q\right)\right]}{\pi B\left(t-\tau_q\right)} \end{aligned} \tag{3}$$

where * represents the convolution operation, $(\cdot)^*$ represents the complex conjugate operation, $B = KT$ is the bandwidth of the transmitted signal and determines the range resolution of the radar system.

In this model, it is assumed that the strong scattering point cannot be distinguished by the range resolution with other weak scattering points. At the same time, strong scattering point sidelobes can also mask weak scattering points.

Note that the scattering points are usually positioned on the non-grid range points, and sidelobes are difficult to suppress by the classical APC algorithms.

3. Methods

When dealing with dense targets, sidelobes of the multiple targets are a challenge for effectively mitigating pulse compression. It becomes imperative to conduct an analysis of the echo and accurately ascertain the locations of non-grid scattering points of the target. Consequently, the suppression of high sidelobes can be achieved based on these estimated positions.

In this section, the target model with non-grid multiple scattering points is constructed. Section 3.1 proposes the modified MUSIC algorithm to estimate the time-delay offsets of non-grid multiple scattering points in echo signal. Section 3.2 constructs the non-grid multiple scattering points model according to the delay offset of the targets. The targets' sidelobes are suppressed by employing the distance sidelobe suppression algorithm based on MMSE criterion.

3.1. Scattering Points Offset Estimation Algorithm Based on Modified MUSIC

In the non-grid multiple scattering points model proposed in this paper, the scattering points are located on the non-grid sampling points. Traditional estimation algorithms, such as the maximum likelihood (ML) and window estimation algorithm, are inadequate for accurately estimating and locating non-grid scattering points. Compared with the above two algorithms, the MUSIC algorithm can measure the offsets of multiple scattering points simultaneously with higher accuracy and resolution and has stable and excellent performance.

Classical MUSIC algorithm is based on the principle that echo signal subspace and noise signal subspace are orthogonal when the covariance matrix is full rank. However, the echo signals in this model are coherent. Hence, it is necessary to preprocess the coherent signal using the spatial smoothing technique to modify the MUSIC algorithm for obtaining the correct estimation of the coherent model. The modified MUSIC algorithm ensures the accuracy of the estimation.

In practical applications, the value of τ_l cannot be calculated by direct measurement. Since the linear frequency modulation signal is used in this paper, multiple scattering points superimpose echo signals with different offsets, which makes direct use of MUSIC algorithm unfeasible. Therefore, Dechirp processing is required for echo signals. The single frequency signal corresponding to the multiple scattering points is obtained and then processed by the MUSIC algorithm. The Dechirp reference signal is constructed based on the transmitted signal, $s_{\mathrm{ref}}(t)=\exp\left[-\mathrm{j}\pi K\left(t-\tau_{\mathrm{ref}}\right)^2\right]$, where τ_{ref} is the reference offset.

To obtain the signal after Dechirp processing, the echo signal is multiplied by the reference signal as follows:

$$\begin{aligned} s_{\mathrm{rd}}(t) &= y(t)\times s_{\mathrm{ref}}(t) \\ &= \sum_{q=0}^{Q-1} s_q\left(t,\tau_q\right) \\ &= \sum_{q=0}^{Q-1} \mathrm{rect}\left(\frac{t-\tau_q}{T_{\mathrm{p}}}\right)\exp\left[\mathrm{j}2\pi K\left(\tau_{\mathrm{ref}}-\tau_q\right)t\right]\exp\left[\mathrm{j}\pi K\left(\tau_q^2-\tau_{\mathrm{ref}}^2\right)\right] \end{aligned} \tag{4}$$

We can find that the signal in Equation (4) is processed by multiplying a rectangular window. The length and position of the window are determined based on the length and position of the common part of the multiple scattering points echo signal. The result of multiplying a window is equivalent to truncating the signal containing the q scattering points and the peak point of the signal $\tilde{s}_q\left(t,\tau_q\right)$. This can be expressed as follows:

$$\begin{aligned} \tilde{s}(t) &= \mathrm{rect}\left(\frac{t-t_0}{T_{\mathrm{w}}}\right)s_{\mathrm{rd}}(t) \\ &= \mathrm{rect}\left(\frac{t-t_0}{T_{\mathrm{w}}}\right)\sum_{q=0}^{Q-1} s_q\left(t,\tau_q\right) \\ &= \sum_{q=0}^{Q-1} \tilde{s}_q\left(t,\tau_q\right) \\ \tilde{s}_q\left(t,\tau_q\right) &= \alpha_q \mathrm{rect}\left(\frac{t-t_0}{T_{\mathrm{w}}}\right)\mathrm{rect}\left(\frac{t-\tau_q}{T_{\mathrm{p}}}\right)\exp\left[\mathrm{j}2\pi K\left(\tau_{\mathrm{ref}}-\tau_q\right)t\right]\exp\left[\mathrm{j}\pi K\left(\tau_q^2-\tau_{\mathrm{ref}}^2\right)\right] \end{aligned} \tag{5}$$

where $T_{\mathrm{w}}=L_{\mathrm{w}}/f_{\mathrm{s}}$, L_{w} is the signal's length. The $\exp\left[\mathrm{j}\pi K\left(\tau_q^2-\tau_{\mathrm{ref}}^2\right)\right]$ in Equation (5) is a constant term. Its single frequency is $f_q=K\left(\tau_{\mathrm{ref}}-\tau_q\right)$, where τ_q can be expressed as follows:

$$\tau_q = \tau_{\text{ref}} - f_q / K, q = 1,2,...,Q \tag{6}$$

Since the echo signal has Q scattering points, the Dechirp echo matrix can be constructed according to the τ_q obtained by Equation (6), as shown in Equation (7):

$$\mathbf{G} = \begin{bmatrix} \tilde{s}_0\left(t,\tau_0\right) \\ \tilde{s}_1\left(t,\tau_1\right) \\ \vdots \\ \tilde{s}_{Q-1}\left(t,\tau_{Q-1}\right) \end{bmatrix}^{\mathrm{T}} \tag{7}$$

Therefore, the signal model can be constructed as follows:

$$\mathbf{X} = \mathbf{GS} + \mathbf{N} \tag{8}$$

where $\mathbf{X}$ represents the echo signal vector after Dechirp processing, $\mathbf{G}$ corresponds to a matrix of size $L \times L_{\text{w}}$, which is obtained by intercepting multiple scattering points' Dechirp echo matrix. $\mathbf{S}$ represents the amplitude of the scattering points, and $\mathbf{N}$ corresponds to the noise signal vector. According to Equation (8), the super-resolution of the MUSIC algorithm can be used to determine the specific grid offsets of the scattering points.

Therefore, the covariance matrix of the signal after Dechirp can be written as follows:

$$\mathbf{R_s} = \mathrm{E}\left[\mathbf{X}\mathbf{X}^{\mathbf{H}}\right] \tag{9}$$

The echo signals of the multiple scattering points are coherent. In order to obtain correct estimation of the coherent model, the spatial smoothing technique is used to preprocess the coherent signals. The matrix $\mathbf{R_{xx}}$ is as follows:

$$\mathbf{R_{xx}} = \frac{1}{d}\sum_{j=1}^{d}\mathbf{R_{sj}} \tag{10}$$

where d represents the number of submatrices, $\mathbf{R_{sj}}$ corresponds to the submatrix intercepted by $\mathbf{R_s}$, and $\mathbf{R_{xx}}$ represents the covariance matrix obtained after spatial smoothing and decoherence operation. Singular value decomposition (SVD) is then performed on the covariance matrix $\mathbf{R_{xx}}$, which is as follows:

$$\mathbf{R_{xx}} = \mathbf{USV}^{\mathbf{T}} \tag{11}$$

where the decomposition of $\mathbf{R_{xx}}$ results in an eigenvalue matrix, represented by $\mathbf{S} = \mathrm{diag}\left(\lambda_1, \lambda_2 \ldots, \lambda_M\right)$, and an eigenvector matrix, represented by $\mathbf{U} = \left[u_1, u_2, \ldots u_M\right]$.

$\mathbf{R_{xx}}$ is a semi-positive definite matrix with M eigenvalues, among which Q eigenvalues are positive and $M-Q$ eigenvalues are close to zero. This enables $\mathbf{R_{xx}}$ to be separated into two subspaces: one subspace with Q dimension representing the signal space, and the other subspace with $M-Q$ dimension representing the noise signal space.

To obtain the precise non-grid offsets, the time-delay grid is divided near the peak point, and each grid is subdivided Z times to construct a subdivided Dechirp matrix, represented by $\boldsymbol{G}$.

To obtain the precise non-grid offsets, intercept part of the signal with length 10 before and after the peak point, refine the time axis of this signal to Z times of the sampling rate, then construct a subdivided Dechirp matrix $\boldsymbol{G}$.

The spatial spectral function P_{MUSIC} can be written as follows:

$$P_{\mathrm{MUSIC}}\left(p_q\right)=\frac{1}{a^{\mathrm{H}}\left(p_q\right)\mathbf{USV}^{\mathrm{H}}a\left(p_q\right)} \tag{12}$$

The non-grid offsets subdivision point corresponding to the maximum value of P_{MUSIC} is used to determine the position $p=\left[p_0,p_1,...,p_{Q-1}\right]$. The position information of scattering points can be determined with an accuracy of up to two decimal places. The specific positions of the non-grid scattering points can be obtained through the following calculation: the offsets between the grid point positions and their non-grid point, which gives rise to specific positions P and the non-grid delay offsets $\boldsymbol{\Delta}$. These are given by the following:

$$\begin{aligned}\boldsymbol{\Delta}&=\frac{Z}{L}-\left\lfloor\frac{Z}{L}\right\rfloor\\ P_q&=l+\Delta_q\end{aligned} \tag{13}$$

where Q represents the number of scattering points. $\lfloor\cdot\rfloor$ represents the rounding function, $P=\left[P_0,P_1,...,P_{Q-1}\right]$ represents the specific positions of scattering points, while P_q represents the specific position of the non-grid scattering point after adding the offset on the grid point, which is accurate to two decimal places. The non-grid offset of the signal is denoted by $\boldsymbol{\Delta}=\left[\Delta_0,\Delta_1,\ldots,\Delta_{Q-1}\right]^{\mathrm{T}},\Delta_q\in\left(-0.5,0.5\right]$. The flow chart of MUSIC algorithm is shown in Figure 1.

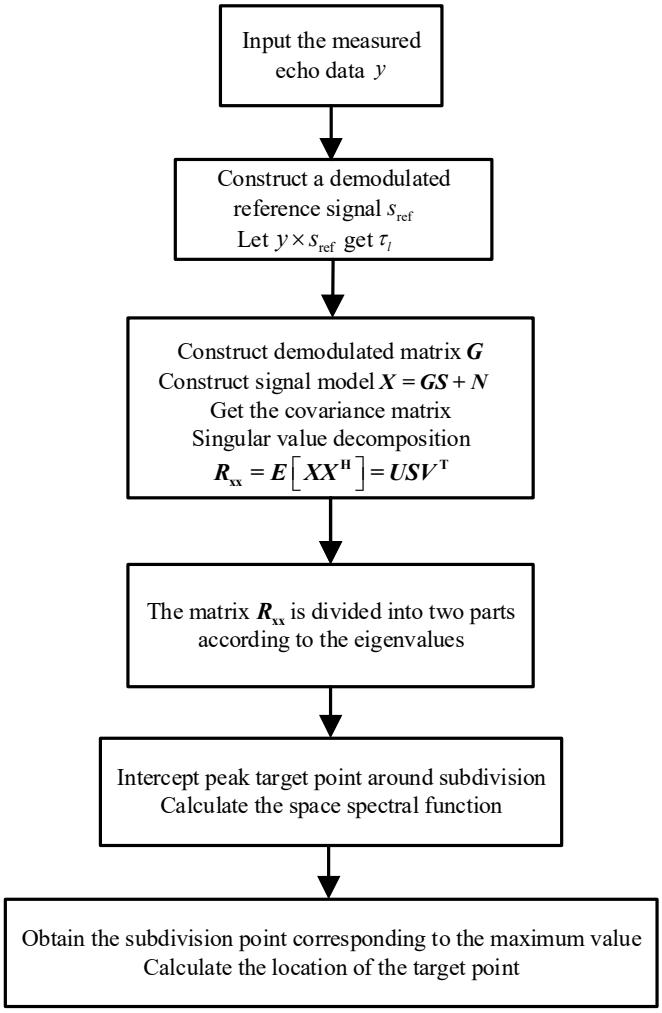

Figure 1. Flow chart of target scattering points offset estimation algorithm based on modified MUSIC.

3.2. Target Sidelobe Iterative Suppression Algorithm Based on Non-Grid Model

The non-grid offsets $\Delta_q (q = 1, 2, ..., Q)$ obtained by the MUSIC algorithm can be used to determine the delay $\tau_q = lT_s + \Delta_q$ of the target point at the range unit l, where T_s represents the sampling time interval, let $t = nT_s$, $T_s = 1/f_s$, and f_s represents the sampling frequency. Under this sampling condition, the signal model can be converted into a vector form to obtain the frequency modulation signal sequence $\boldsymbol{s}$, which is as follows:

$$\boldsymbol{s} = \left[s(0), s(1), \ldots, s(N-1) \right]^{\mathrm{T}} \tag{14}$$

where N represents the number of sampling points within a pulse width.

The radar echo signal model of the scattering point q at the range unit l after being sampled is given by the following:

$$\begin{aligned} \tilde{y}(l, \Delta_q) &= \boldsymbol{x}^{\mathrm{T}}(l, \Delta_q) \boldsymbol{s} \odot \boldsymbol{e}(\Delta_q) + \tilde{v}(l) \\ &= \boldsymbol{x}^{\mathrm{T}}(l, \Delta_q) \tilde{\boldsymbol{s}}(\Delta_q) + \tilde{v}(l) \end{aligned} \tag{15}$$

where $\boldsymbol{x}(l, \Delta_q) = \left[x(l, \Delta_q), x(l-1, \Delta_q), ..., x(l-N, \Delta_q) \right]^{\mathrm{T}}$ represents N-point continuous sampling when the qth scattering point is non-grid, and $\tilde{v}(l)$ is additive Gaussian white noise vector. $\odot$ represents the Hadamard product, $\boldsymbol{e}(\Delta_q) = \left[\mathrm{e}^{\mathrm{j}g(\Delta_q)}, \mathrm{e}^{\mathrm{j}g(T_s + \Delta_q)}, ..., \mathrm{e}^{\mathrm{j}g((N-1)T_s + \Delta_q)} \right]^{\mathrm{T}}$ represents the phase mismatch between the linear frequency modulation signal and the grid point caused by Δ_q, and $g(\cdot)$ represents the frequency modulation function of the signal.

The pulse compression output of the matched filter after sampling at the qth scattering point is obtained by convolving the complex conjugate of the transmitted signal with the echo, and is expressed in discrete form as follows:

$$\begin{aligned} x_{\mathrm{MF}}(l, \Delta_q) &= \tilde{\boldsymbol{s}}^{\mathrm{H}}(\Delta_q) \tilde{\boldsymbol{y}}(l, \Delta_q) \\ &= \tilde{\boldsymbol{s}}^{\mathrm{H}}(\Delta_q) \boldsymbol{A}^{\mathrm{T}}(l, \Delta_q) \tilde{\boldsymbol{s}}(\Delta_q) + \tilde{\boldsymbol{s}}^{\mathrm{H}}(\Delta_q) \tilde{\boldsymbol{v}}(l) \end{aligned} \tag{16}$$

where $\tilde{\boldsymbol{y}}(l, \Delta_q) = \left[\tilde{y}(l, \Delta_q), \tilde{y}(l+1, \Delta_q), ..., \tilde{y}(l+N-1, \Delta_q) \right]^{\mathrm{T}}$ represents N-point continuous sampling of the echo pulse corresponding to the range unit l when sampling mismatch occurs. Its specific expression is given by the following:

$$\tilde{\boldsymbol{y}}(l, \Delta_q) = \boldsymbol{A}^{\mathrm{T}}(l, \Delta_q) \tilde{\boldsymbol{s}}(\Delta_q) + \tilde{\boldsymbol{v}}(l) \tag{17}$$

where $\boldsymbol{A}(l, \Delta_q) = \left[\boldsymbol{x}(l, \Delta_q), \boldsymbol{x}(l+1, \Delta_q), ..., \boldsymbol{x}(l+N-1, \Delta_q) \right]$ is the N-point continuous sampling matrix of distance dimension when the q th scattering point is non-grid, and $\tilde{\boldsymbol{v}}(l) = \left[\tilde{v}(l), \tilde{v}(l+1), ..., \tilde{v}(l+N-1) \right]$ is the noise vector.

The previous item of the matched filter output $x_{\mathrm{MF}}(l, \Delta_q)$ can be expressed as follows:

$$
\begin{aligned}
\boldsymbol{s}^{\mathrm{H}}\left(\Delta_q\right)\boldsymbol{A}^{\mathrm{T}}\left(l,\Delta_q\right)\boldsymbol{s}\left(\Delta_q\right) &= \boldsymbol{s}^{\mathrm{H}}\left(\Delta_q\right)\begin{bmatrix}\boldsymbol{x}^{\mathrm{T}}\left(l,\Delta_q\right)\\ \boldsymbol{x}^{\mathrm{T}}\left(l+1,\Delta_q\right)\\ \vdots\\ \boldsymbol{x}^{\mathrm{T}}\left(l+N-1,\Delta_q\right)\end{bmatrix}\boldsymbol{s}\left(\Delta_q\right)\\
&= \boldsymbol{s}^{\mathrm{H}}\left(\Delta_q\right)\begin{bmatrix}\boldsymbol{s}^{\mathrm{T}}\boldsymbol{x}\left(l,\Delta_q\right)\\ \boldsymbol{s}^{\mathrm{T}}\boldsymbol{x}\left(l+1,\Delta_q\right)\\ \vdots\\ \boldsymbol{s}^{\mathrm{T}}\boldsymbol{x}\left(l+N-1,\Delta_q\right)\end{bmatrix}\\
&= \boldsymbol{s}^{\mathrm{H}}\left(\Delta_q\right)\begin{bmatrix}0 & \cdots & 0 & s_0\left(\Delta_q\right)\\ \vdots & & \iddots & s_1\left(\Delta_q\right)\\ 0 & s_0\left(\Delta_q\right) & & \vdots\\ s_0\left(\Delta_q\right) & s_1\left(\Delta_q\right) & \cdots & s_{N-1}\left(\Delta_q\right)\\ s_1\left(\Delta_q\right) & \vdots & \iddots & 0\\ \vdots & s_{N-1}\left(\Delta_q\right) & & \vdots\\ s_{N-1}\left(\Delta_q\right) & & & 0\end{bmatrix}^{\mathrm{T}}\hat{\boldsymbol{x}}\left(l,\Delta_q\right)\\
&= \boldsymbol{s}^{\mathrm{H}}\left(\Delta_q\right)\tilde{\boldsymbol{S}}^{\mathrm{T}}\left(\Delta_q\right)\hat{\boldsymbol{x}}\left(l,\Delta_q\right)
\end{aligned}
\tag{18}
$$

where $\hat{\boldsymbol{x}}\left(l,\Delta_q\right)=\left[x\left(l+N-1,\Delta_q\right)\ \cdots\ x\left(l,\Delta_q\right)\ \cdots\ x\left(l-N+1,\Delta_q\right)\right]^{\mathrm{T}}$, let $\tilde{\boldsymbol{S}}\left(\Delta_q\right)\boldsymbol{s}^{*}\left(\Delta_q\right)=\hat{\boldsymbol{r}}\left(\Delta_q\right)$, $\hat{\boldsymbol{r}}\left(\Delta_q\right)=\left[r_{-N+1}\left(\Delta_q\right)\ \cdots\ r_0\left(\Delta_q\right)\ \cdots\ r_{N-1}\left(\Delta_q\right)\right]^{\mathrm{T}}$ be the autocorrelation function of the reference transmitted signal $\boldsymbol{s}\left(\Delta_q\right)$.

Then, the range unit l matched by the qth scattering point after filtering can be expressed as follows:

$$
x_{\mathrm{MF}}\left(l,\Delta_q\right)=\hat{\boldsymbol{x}}^{\mathrm{T}}\left(l,\Delta_q\right)\hat{\boldsymbol{r}}\left(\Delta_q\right)+u\left(l\right) \tag{19}
$$

Using the pulse compression technique, most of the energy of the target concentrated in several range units allows for the application of processing windows in the construction of filter coefficients and reduces computation. The $\bar{x}_{\mathrm{MF}}\left(l,\Delta_q\right)$ calculated through the processing window can be expressed as follows:

$$
\bar{x}_{\mathrm{MF}}\left(l,\Delta_q\right)=\tilde{\boldsymbol{x}}^{\mathrm{T}}\left(l,\Delta_q\right)\tilde{\boldsymbol{r}}\left(\Delta_q\right)+u\left(l\right) \tag{20}
$$

where $\tilde{\boldsymbol{x}}\left(l,\Delta_q\right)=\left[x\left(l+K_{\mathrm{d}},\Delta_q\right)\ \cdots\ x\left(l,\Delta_q\right)\ \cdots\ x\left(l-K_{\mathrm{r}},\Delta_q\right)\right]^{\mathrm{T}}$, $\tilde{\boldsymbol{r}}=\left[r_{-K_{\mathrm{r}}}\left(\Delta_q\right)\ \cdots\ r_0\left(\Delta_q\right)\ \cdots\ r_{K_{\mathrm{d}}}\left(\Delta_q\right)\right]^{\mathrm{T}}$.

Then, the sampling value of $K_{\mathrm{r}}+K_{\mathrm{d}}+1$ point matched by the qth scattering point can be expressed as follows:

$$
\boldsymbol{x}_{\mathrm{MF}}\left(l,\Delta_q\right)=\boldsymbol{B}^{\mathrm{T}}\left(l,\Delta_q\right)\tilde{\boldsymbol{r}}\left(\Delta_q\right)+\tilde{\boldsymbol{u}}\left(l\right) \tag{21}
$$

where $\boldsymbol{x}_{\mathrm{MF}}\left(l,\Delta_q\right)=\left[\bar{x}_{\mathrm{MF}}\left(l-K_{\mathrm{r}},\Delta_q\right),\bar{x}_{\mathrm{MF}}\left(l-K_{\mathrm{r}}+1,\Delta_q\right)...,\ \bar{x}_{\mathrm{MF}}\left(l+K_{\mathrm{d}},\Delta_q\right)\right]$, $\tilde{\boldsymbol{u}}\left(l\right)=\left[u\left(l-K_{\mathrm{r}}\right)\ \cdots\ u\left(l\right)\ \cdots\ u\left(l+K_{\mathrm{d}}\right)\right]^{\mathrm{T}}$.

$$\begin{aligned}\boldsymbol{B}\left(l,\Delta_q\right)&=\left[\tilde{\boldsymbol{x}}\left(l-K_{\mathrm{r}},\Delta_q\right)\quad\tilde{\boldsymbol{x}}\left(l-K_{\mathrm{r}}+1,\Delta_q\right)\Delta_q\quad\cdots\quad\tilde{\boldsymbol{x}}\left(l+K_{\mathrm{d}},\Delta_q\right)\right]\\&=\begin{bmatrix}x\left(l-K_{\mathrm{r}}+K_{\mathrm{d}},\Delta_q\right)&\cdots&x\left(l+2K_{\mathrm{d}},\Delta_q\right)\\\vdots&\ddots&\vdots\\x\left(l-2K_{\mathrm{r}},\Delta_q\right)&\cdots&x\left(l-K_{\mathrm{r}}+K_{\mathrm{d}},\Delta_q\right)\end{bmatrix}\end{aligned}\tag{22}$$

Echo signal model $\tilde{\boldsymbol{y}}\left(l,\Delta_q\right)$ and its pulse compression signal model $\boldsymbol{x}_{\mathrm{MF}}\left(l,\Delta_q\right)$ were constructed according to the non-grid offset Δ_q of range unit l calculated by the above algorithm.

In the process of non-grid APC processing on the pulse compression signal, when the non-grid scattering points estimated by the MUSIC algorithm are processed, in order to develop MMSE filter on the signal model of the non-grid points, the cost function is designed by using the MF signal model.

Based on RMMSE criterion, the cost function is constructed by using the output result of matching filter, the cost function is as follows:

$$\boldsymbol{J}\left(l\right)=\sum_{q=0}^{Q-1}\mathrm{E}\left[\left|x\left(l,\Delta_q\right)-\boldsymbol{\omega}^{\mathrm{H}}\left(l\right)\boldsymbol{x}_{\mathrm{MF}}\left(l,\Delta_q\right)\right|^2\right]\tag{23}$$

where $\mathrm{E}[\cdot]$ represents the statistical expectation, and $\boldsymbol{\omega}(l)$ is a $\left(K_{\mathrm{r}}+K_{\mathrm{d}}+1\right)\times 1$ size of MMSE filtering coefficient vector, which is the unique calculation of signal amplitude $x(l)$ for each individual non-grid scattering points cell. $K=K_{\mathrm{r}}+K_{\mathrm{d}}+1$ is the length of MMSE filter.

If $\boldsymbol{J}(l)$ take the gradient with respect to $\boldsymbol{\omega}^{\mathrm{H}}(l)$ and set it to zero, that is the following:

$$\nabla_{\boldsymbol{\omega}^{\mathrm{H}}}\boldsymbol{J}\left(\boldsymbol{\omega},\boldsymbol{\omega}^{\mathrm{H}}\right)=0\tag{24}$$

which can be calculated as follows:

$$\nabla_{\boldsymbol{\omega}^{\mathrm{H}}}\boldsymbol{J}\left(\boldsymbol{\omega},\boldsymbol{\omega}^{\mathrm{H}}\right)=\sum_{q=0}^{Q-1}\mathrm{E}\left\{\boldsymbol{x}_{\mathrm{MF}}\left(l,\Delta_q\right)x^{*}\left(l,\Delta_q\right)-\boldsymbol{x}_{\mathrm{MF}}\left(l,\Delta_q\right)\boldsymbol{x}_{\mathrm{MF}}^{\mathrm{H}}\left(l,\Delta_q\right)\boldsymbol{\omega}\left(l\right)\right\}=0\tag{25}$$

it is equivalent to the following:

$$\boldsymbol{\omega}\left(l\right)=\sum_{q=0}^{Q-1}\left\{\mathrm{E}\left[\boldsymbol{x}_{\mathrm{MF}}\left(l,\Delta_q\right)\boldsymbol{x}_{\mathrm{MF}}^{\mathrm{H}}\left(l,\Delta_q\right)\right]\right\}^{-1}\mathrm{E}\left[\boldsymbol{x}_{\mathrm{MF}}\left(l,\Delta_q\right)x^{*}\left(l,\Delta_q\right)\right]\tag{26}$$

If the impulse response of each range unit is not correlated, that is when $\mathrm{E}\left[x(m)x(n)\right]=0,\ m\neq n$, and independent from noise statistics, that is $\mathrm{E}\left[x(m)v(n)\right]=0$, then we can obtain the following:

$$\begin{aligned}\mathrm{E}\left[\boldsymbol{x}_{\mathrm{MF}}\left(l\right)\boldsymbol{x}_{\mathrm{MF}}^{\mathrm{H}}\left(l\right)\right]&=\sum_{q=0}^{Q-1}\mathrm{E}\left[\boldsymbol{B}^{\mathrm{T}}\left(l,\Delta_q\right)\tilde{\boldsymbol{r}}\left(\Delta_q\right)\tilde{\boldsymbol{r}}^{\mathrm{T}}\left(\Delta_q\right)\boldsymbol{B}\left(l,\Delta_q\right)\right]+\tilde{\boldsymbol{R}}\\&=\sum_{q=0}^{Q-1}\sum_{n=-2K_{\mathrm{r}}}^{2K_{\mathrm{d}}}\tilde{\rho}\left(l+n\right)\tilde{\boldsymbol{r}}_n\left(\Delta_q\right)\tilde{\boldsymbol{r}}_n^{\mathrm{T}}\left(\Delta_q\right)+\tilde{\boldsymbol{R}}\\&=\sum_{q=0}^{Q_1-1}\sum_{n=-2K_{\mathrm{r}}}^{2K_{\mathrm{d}}}\rho\left(l+n,\Delta_q\right)\tilde{\boldsymbol{r}}_n\left(\Delta_q\right)\tilde{\boldsymbol{r}}_n^{\mathrm{T}}\left(\Delta_q\right)+\sum_{q=0}^{Q_2-1}\sum_{n=-2K_r}^{2K_d}\rho\left(l+n\right)\tilde{\boldsymbol{r}}_n\tilde{\boldsymbol{r}}_n^{\mathrm{T}}+\tilde{\boldsymbol{R}}\end{aligned}\tag{27}$$

$$\begin{aligned}\mathrm{E}\left[\boldsymbol{x}_{\mathrm{MF}}\left(l,\Delta_q\right)x^*\left(l,\Delta_q\right)\right]&=\sum_{q=0}^{Q-1}\mathrm{E}\left[\boldsymbol{B}^{\mathrm{T}}\left(l,\Delta_q\right)x^*\left(l,\Delta_q\right)\right]\tilde{\boldsymbol{r}}\left(\Delta_q\right)\\&=\sum_{q=0}^{Q-1}\tilde{\rho}(l)\boldsymbol{I}_{K_{\mathrm{r}}+K_{\mathrm{d}}+1}\tilde{\boldsymbol{r}}\left(\Delta_q\right)\\&=\sum_{q=0}^{Q_1-1}\rho\left(l,\Delta_q\right)\boldsymbol{I}_{K_{\mathrm{r}}+K_{\mathrm{d}}+1}\tilde{\boldsymbol{r}}\left(\Delta_q\right)+\sum_{q=0}^{Q_2-1}\rho(l)\boldsymbol{I}_{K_{\mathrm{r}}+K_{\mathrm{d}}+1}\tilde{\boldsymbol{r}}\end{aligned}\tag{28}$$

where $\rho\left(l,\Delta_q\right)=\left|x\left(l,\Delta_q\right)\right|^2$ represents the expected power of $x\left(l,\Delta_q\right)$, $\rho(l)=\left|x(l)\right|^2$ represents the expected power of $x(l)$, $\boldsymbol{I}_{K_{\mathrm{r}}+K_{\mathrm{d}}+1}$ is the identity matrix of $(K_{\mathrm{r}}+K_{\mathrm{d}}+1)\times(K_{\mathrm{r}}+K_{\mathrm{d}}+1)$ dimension, $\tilde{\boldsymbol{R}}=\mathrm{E}\left[\tilde{\boldsymbol{u}}(l)\tilde{\boldsymbol{u}}^{\mathrm{H}}(l)\right]$ represents the noise covariance matrix of size $(K_{\mathrm{r}}+K_{\mathrm{d}}+1)\times(K_{\mathrm{r}}+K_{\mathrm{d}}+1)$, so we can obtain the $\boldsymbol{\omega}(l)$ as follows:

$$\boldsymbol{\omega}(l)=\tilde{\rho}(l)\left(\boldsymbol{C}(l)+\tilde{\boldsymbol{R}}\right)^{-1}\tilde{\boldsymbol{r}}\left(\Delta_q\right)\tag{29}$$

$$\boldsymbol{C}(l)=\sum_{q=0}^{Q_1-1}\sum_{n=-2K_{\mathrm{r}}}^{2K_{\mathrm{d}}}\rho\left(l+n,\Delta_q\right)\tilde{\boldsymbol{r}}_n\left(\Delta_q\right)\tilde{\boldsymbol{r}}_n^{\mathrm{T}}\left(\Delta_q\right)+\sum_{q=0}^{Q_2-1}\sum_{n=-2K_{\mathrm{r}}}^{2K_{\mathrm{d}}}\rho(l+n)\tilde{\boldsymbol{r}}_n\tilde{\boldsymbol{r}}_n^{\mathrm{T}}\tag{30}$$

where $\tilde{\boldsymbol{r}}_n\left(\Delta_q\right)$ means to shift the signal $\tilde{\boldsymbol{r}}\left(\Delta_q\right)$ by n bits, leaving a blank bit to fill in the zero. For example, when $n=2$, $\tilde{\boldsymbol{r}}_2\left(\Delta_q\right)=\left[0\quad 0\quad r_{-K_{\mathrm{r}}}\left(\Delta_q\right)\quad\cdots\quad r_{K_{\mathrm{d}}-2}\left(\Delta_q\right)\right]^{\mathrm{T}}$, when $n=-2$, $\tilde{\boldsymbol{r}}_{-2}\left(\Delta_q\right)=\left[r_{-K_{\mathrm{r}}+2}\left(\Delta_q\right)\quad\cdots\quad r_{K_{\mathrm{d}}}\left(\Delta_q\right)\quad 0\quad 0\right]^{\mathrm{T}}$.

To calculate the filter coefficient $\boldsymbol{\omega}(l)$ of the range unit l according to Equations (27) and (28), prior information of the output power of the unit before and after the grid point is required. After obtaining the filter coefficient $\boldsymbol{\omega}(l)$, it is conjugate transposed in order to suppress the sidelobe at the range unit l. The flow chart of the target sidelobes iterative suppression algorithm based on the non-grid model is shown in Figure 2.

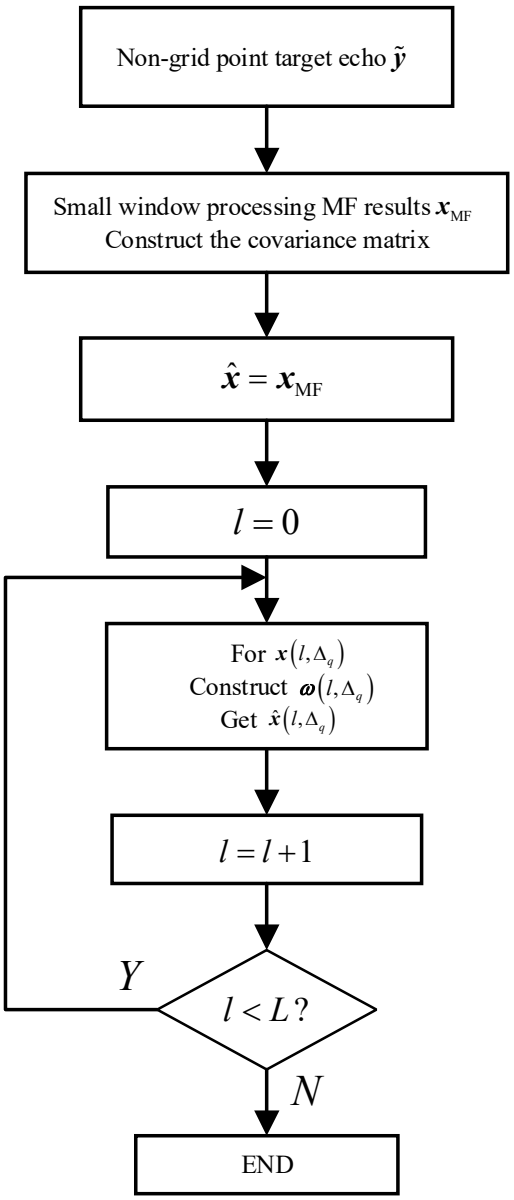

Figure 2. Flow chart of target sidelobe iterative suppression algorithm based on non-grid model.

3.3. Computational Complexity Analysis

The range dimension sidelobes suppression algorithm based on non-grid scattering points echo signal differs from that based on grid point echo signal by accounting for non-grid issues in practical applications. The distance dimension sidelobes suppression algorithm based on non-grid scattering points echo signal is introduced, and the reference template is adjusted according to the offsets to reduce the computational complexity of the algorithm using a small processing window.

The detailed implementation steps of these two algorithms are provided in Tables 1 and 2, based on the discussion of the small window non-grid APC processing flow using both echo and matched filter output.

Table 1. Implementation steps of APC algorithm based on echo.

1. Initialization: $\boldsymbol{\omega}^{(0)} = \boldsymbol{s}$, the matched filter output $\boldsymbol{x}_{\mathrm{MF}}$ was calculated by $\hat{x}_{MF}(l) = \mathbf{s}^H \tilde{\mathbf{y}}(l) = \mathbf{s}^H \mathbf{A}^T(l)\mathbf{s} + \mathbf{s}^H \mathbf{v}(l)$, let $i = 1$, $\hat{\boldsymbol{x}}^{(0)} = \boldsymbol{x}_{\mathrm{MF}}$;
2. Calculate power estimates $\rho^{(i)}(l) = \left|\hat{x}^{(i-1)}(l)\right|^2$, and $\boldsymbol{C}^{(i)}(l)$ matrix is constructed by $\mathbf{C}(l) = \sum_{n=-N+1}^{N-1} \rho(l+n)\mathbf{s}_n \mathbf{s}_n^H$;
3. Calculate $\boldsymbol{\omega}^{(i)}(l)$ matrix by $\boldsymbol{\omega}(l) = \rho(l)\left(\mathbf{C}(l) + \mathbf{R}\right)^{-1}\mathbf{s}$;
4. Update $\hat{x}^{(i)}(l)$ by $\hat{x}(l) = \boldsymbol{\omega}^H(l)\tilde{\mathbf{y}}(l)$;
5. Repeat Step 2 until the desired accuracy is achieved.

Table 2. Implementation steps of small-window non-grid APC algorithm based on matched filter output.

1. Initialization: Calculate the matched filter output $\boldsymbol{x}_{\mathrm{MF}}$, let $i = 1$, $\hat{\boldsymbol{x}}^{(0)} = \boldsymbol{x}_{\mathrm{MF}}$;
2. The $\boldsymbol{\Delta}$ is calculated using Equation (13), calculate power estimates $\rho^{(i)}(l) = \left|\hat{x}^{(i-1)}(l)\right|^2$, $\rho^{(i)}(l, \Delta_l) = \left|\hat{x}^{(i-1)}(l, \Delta_l)\right|^2$ and $\boldsymbol{C}^{(i)}(l)$ matrix is constructed by Equation (30);
3. Calculate $\boldsymbol{\omega}^{(i)}(l)$ matrix by Equation (29);
4. Update $\hat{x}^{(i)}(l)$ by $\hat{x}(l) = \tilde{\boldsymbol{\omega}}(l)\mathbf{x}_{MF}(l)$;
5. Repeat Step 2 until the desired accuracy is achieved.

The computational complexity of these two algorithms is analyzed below in Table 3:

Table 3. The computational complexity of each range unit in each iteration.

Steps	Echo APC	Match the Filtered Non-Grid APC
$C(l)$ matrix construction	$(2N-1)N^2$	$2\left(\left(K_{\mathrm{r}}+K_{\mathrm{d}}+1\right)^3 - \left(K_{\mathrm{r}}+K_{\mathrm{d}}+1\right)^2\right)$
Filter weight vector	$N^3 + N^2$	$\left(K_{\mathrm{r}}+K_{\mathrm{d}}+1\right)^3 + \left(K_{\mathrm{r}}+K_{\mathrm{d}}+1\right)^2$
Distance cell $x(l)$ estimation	N	$K_{\mathrm{r}}+K_{\mathrm{d}}+1$

Table 3 displays the computational complexity of the APC algorithm based on echo and the non-grid APC algorithm based on matched filter output with small window, as analyzed below. The complexity of the APC algorithm based on echo is $O\left(N^3\right)$, while that of the non-grid APC algorithm based on matched filter output with small window is $O\left(K^3\right)$, where $K_{\mathrm{w}} = K_{\mathrm{r}} + K_{\mathrm{d}} + 1$. Figure 3 compares the computational complexity of the adaptive pulse compression algorithm based on echo and matched filter. Figure 3 indicates that for $N / K > 5$, the small window treatment can reduce computation by at least two orders of magnitude.

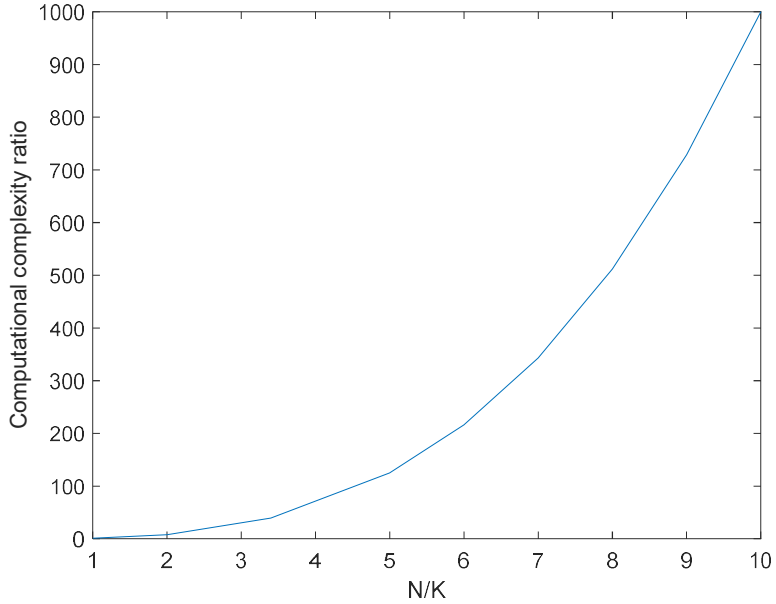

Figure 3. Comparison of computational complexity of algorithm based on echo and MF.

After comparing the echo-based and MF-based APC algorithms, we show that the complexity of the new algorithm is two orders of magnitude lower than that of the echo-based APC algorithm. The comparison with other algorithms is provided in the following Table 4.

Table 4. Comparison of the complexity of each algorithm.

Algorithm	Computational Complexity
APC algorithm based on echo	$O\left(N^3\right)$
FAPC	$O\left(N \log N\right)$
LCMV-APC	$O\left(N^2 N_p\right)$
Non-grid APC	$O\left(K^3\right)$

From Table 4, it is evident that the proposed algorithm exhibits a lower computational complexity compared to the traditional APC algorithm, as well as FAPC and LCMV-APC. This highlights the computational superiority of the proposed algorithm.

4. Results

In both simulation and field tests, the LFM signal is used as the radar transmitting signal. In Section 3.1, multiple scattering points are set and the MUSIC algorithm is used to modify the echo signal to estimate and verify the number and positions of scattering points. In Section 3.2, the scattering points in the echo signal with an unclear number of targets are estimated and their positions are computed. The signal model is constructed to process the suppressed sidelobes of the MF signal, and the effectiveness of the algorithm proposed is verified in this section.

4.1. Simulation Result

For the simulation test, the signal parameters were set as follows: bandwidth $B = 4\text{MHz}$, pulse width $T_\text{p} = 20\mu\text{s}$, sampling frequency $f_\text{s} = 5\text{MHz}$, and pulse repetition period PRI which is $T_\text{r} = 744.8\mu\text{s}$. Four points were set, and their location information is provided in Table 5.

Table 5. Table of simulation scenarios.

Targets	The Index of Sampling Points of the Target Distance Dimension	Target SNR/dB
1	931.09	20
2	934.18	40
3	947.42	80
4	939.11	75.56

The positions of the subdivided peak point and scattering points are calculated by inputting the echo signal into the MUSIC algorithm, which obtained the super-resolution results. Figure 4 shows the resulting super-resolution image, where each extreme point indicates the specific position of a peak point or scattering points on the non-grid. The four extreme points in Figure 4 correspond to the position offsets of P_1, P_2, P_3, and P_4, based on the setting results.

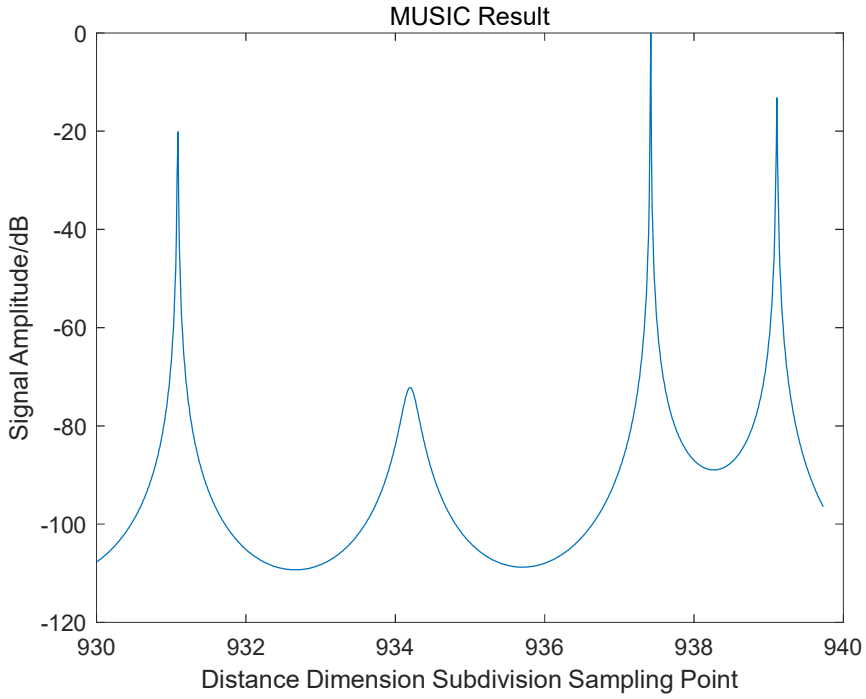

Figure 4. Results of location estimation by multiple points simulation MUSIC algorithm.

The echo signal model is reconstructed using the position information of the scattering points, and the pulse compression signal is calculated as a template. The template and the original pulse compression signal were then input into the adaptive pulse compression algorithm for computation. The results of the algorithm are presented in Figure 5, and the resulting scattering point positions are provided in Table 6.

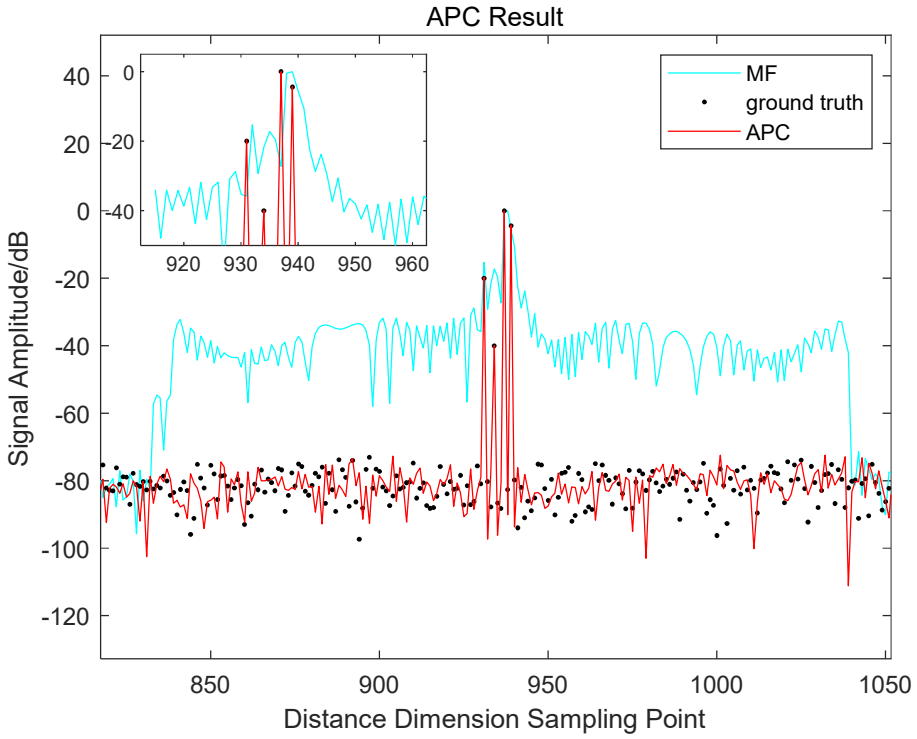

Figure 5. Shows the results of the multi-objective simulation of the non-grid APC algorithm.

Table 6. Simulation results.

Targets	The Index of Sampling Points of the Target Distance Dimension	Ground truth Amplitude/dB	Non-Grid APC Amplitude/dB
1	931.09	−20	−19.65
2	934.18	−40	−39.83
3	947.42	0	0
4	939.11	−4.43	−4.31

From Figure 5 and Table 6, it can be observed that the sidelobes of the signal after applying the non-grid APC algorithm is 60 dB lower than that of the matched filter output result.

In addition, we analyze the processing advantages of the non-grid APC algorithm in the case of non-grid points. The proposed method can probe small targets and distinguish four targets clearly. The corresponding performance is shown in Figures 6 and 7.

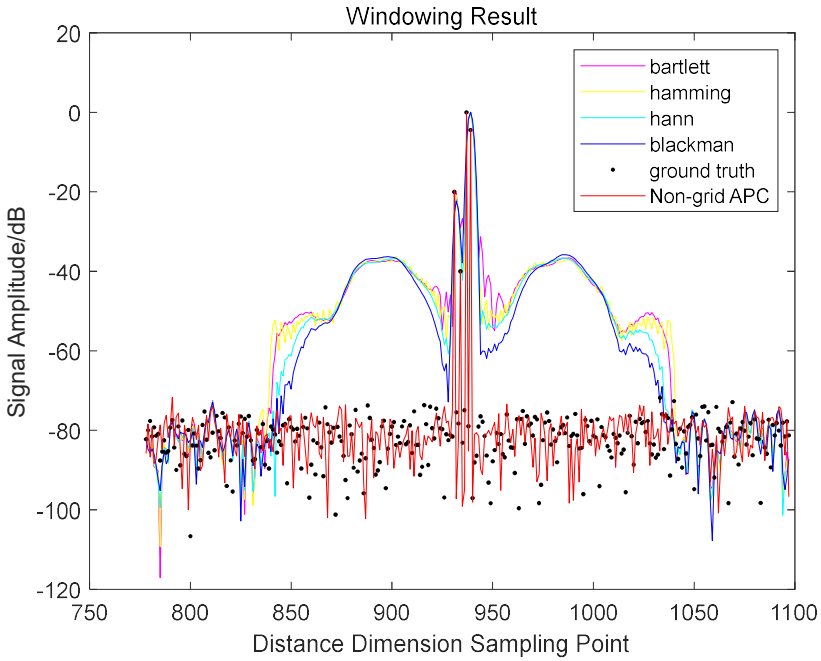

Figure 6. Comparison of windowing algorithm results with non-grid APC algorithm.

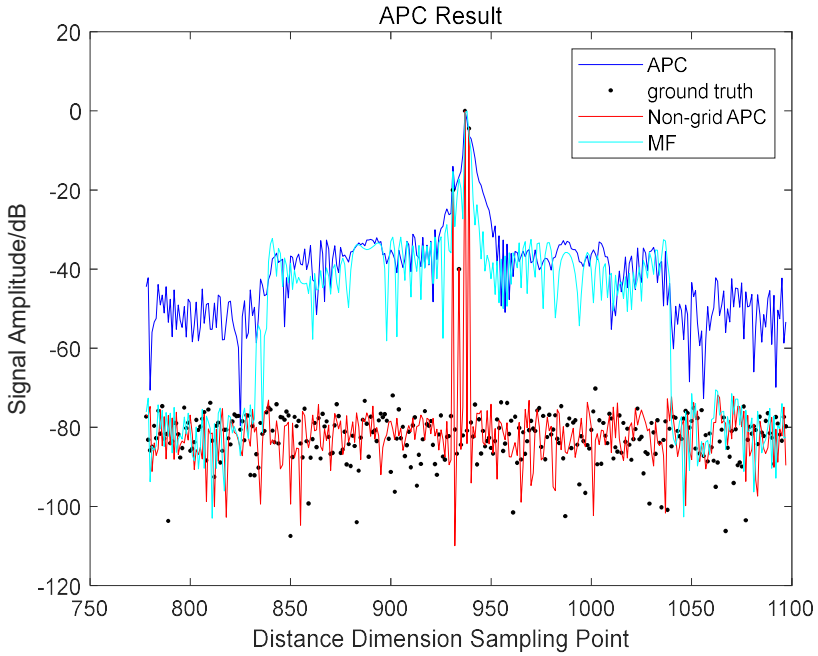

Figure 7. Comparison between traditional grid APC and non-grid APC algorithm.

Figure 6 shows that the windowing algorithm cannot solve the non-grid multiple scatterers problem well. Moreover, it broadens the sidelobes and causes the results to deteriorate. It can be seen from Figure 7 that the adaptive sidelobe suppression technique based on the grid model cannot obtain good sidelobe suppression performance for non-grid multi-scattering targets, while the adaptive sidelobe suppression technique based on the non-grid model can suppress the processing sidelobe to the noise level. The two very near targets cannot be distinguished in the output of MF. However, they can be distinguished by the adaptive sidelobe processing based on the non-mesh model. The weak targets which are masked by the high sidelobes of the MF are also shown by the adaptive sidelobe processing technique based on the non-mesh model. It can be seen from the

figure that the width of the main lobe of the pulse compression signal processed by the adaptive sidelobe suppression algorithm based on the non-grid model is significantly narrower. At the same time, the signal-to-noise ratio loss is very small.

Moreover, the close proximity of the four points causes the sidelobes of the high signal amplitude point to spread over the low signal amplitude points. However, after applying the proposed non-grid sidelobe suppression algorithm, the sidelobes of all points are effectively suppressed. Compared with counterparts, the proposed algorithm is more efficient, with low computational amount and fast processing speed.

4.2. Experimental Results of Tested Data

The tested data, which is measured by radar, have a bandwidth $B = 4\text{MHz}$, a pulse width $T_p = 20\mu\text{s}$, a sampling frequency $f_s = 5\text{MHz}$, and a pulse repetition period PRI which is $T_r = 744.8\mu\text{s}$. Substituting the echo signal into the MUSIC algorithm, the resulting super-resolution image is shown in Figure 8, which was used to calculate the positions of the subdivided peak point and scattering points.

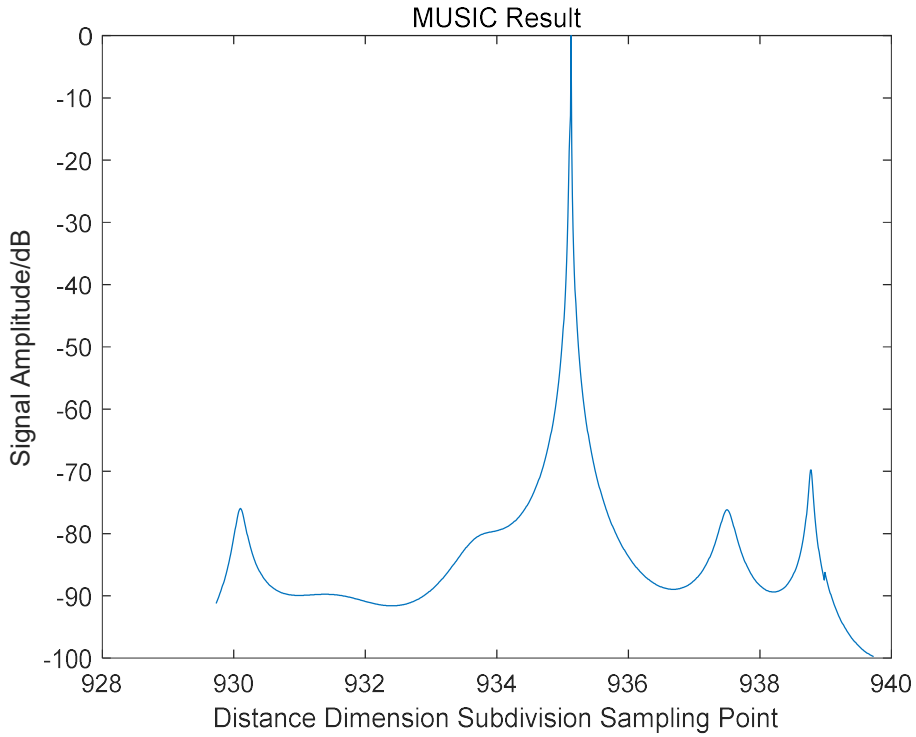

Figure 8. Location estimation results of MUSIC algorithm for tested data.

Figure 8 presents the super-resolution image, with each extreme point indicating the precise position of the peak point and scattering points on the non-grid, which are located at 938.83, 937.45, 935.11, 933.41, and 930.55. Additionally, the echo signal model is reconstructed based on the targets' positions, and a pulse compression signal was calculated as a template. After substituting the resultant signal and the original pulse compression signal into the non-grid APC algorithm, a comparison between the non-grid APC and the original matched filter result is presented in Figure 9.

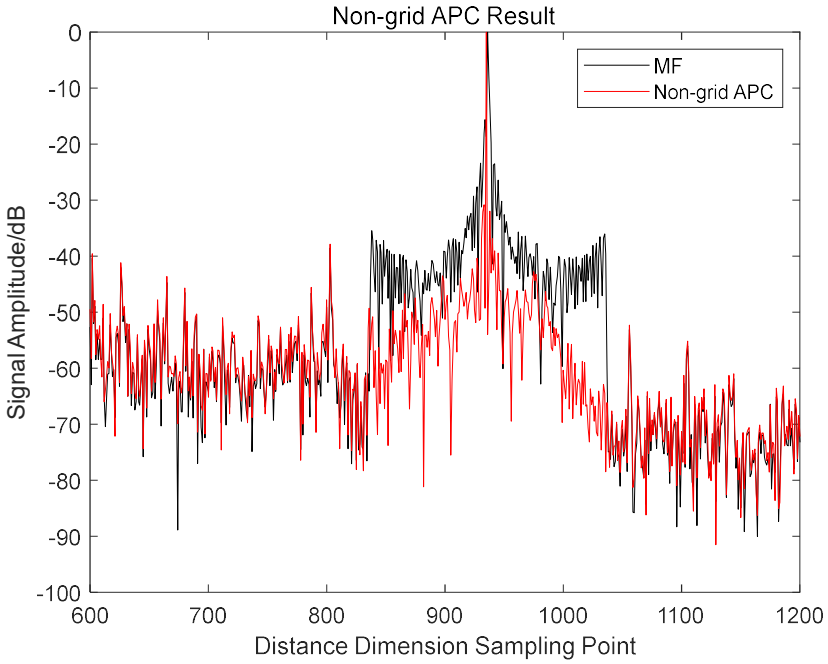

Figure 9. Results of sidelobe suppression by non-grid APC algorithm based on tested data.

Figure 9 shows that the sidelobes are reduced by almost 20 dB with the implementation of the non-grid APC algorithm in comparison to the traditional MF method. The proposed non-grid APC algorithm enables effective suppression of the sidelobes when scattering points' positions and peak signal coordinates are estimated well.

We apply the non-grid APC algorithm to conduct batch processing experiments on 190 groups of tested signals, and the processing results are shown in Figure 10. The figure shows that the proposed algorithm effectively suppresses sidelobe waves for two-dimensional signals.

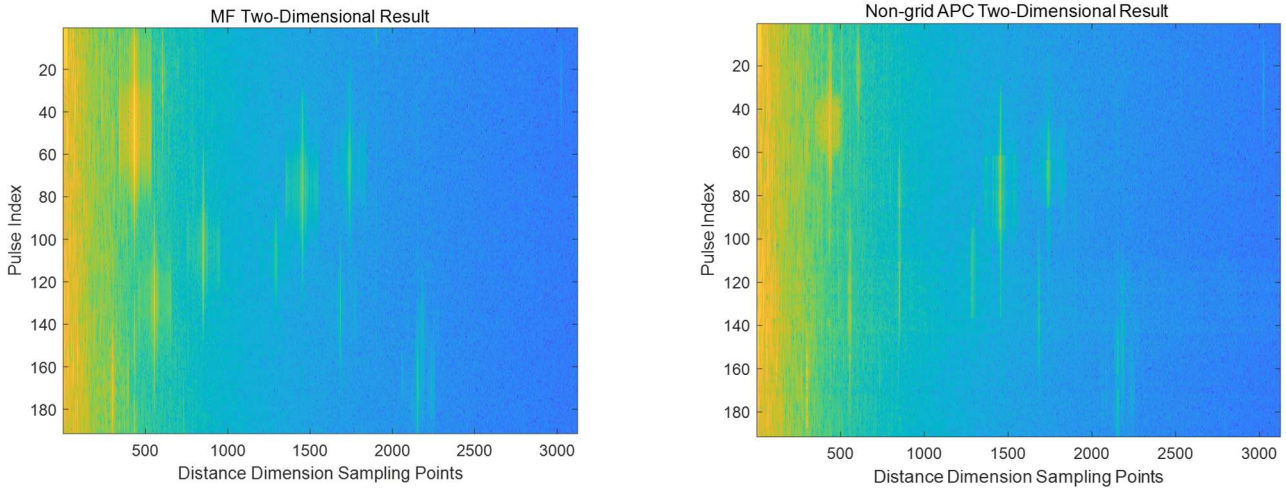

(**a**) (**b**)

Figure 10. Comparison of pulse-by-pulse sidelobe suppression processing in sea surface multiple targets radar beam scanning: (**a**) matching processing; (**b**) sidelobe suppression processing.

In Figure 10, the abscissa represents the sampling points in the distance dimension, and the ordinate represents the pulse index; the sea ship targets are vertically connected into an area. As shown in Figure 10a, the highlighted yellow area represents the peak point

of the scattering points, and the left and right sub-bright light yellow areas represent the weak scattering points and sidelobes. The proposed method suppresses the sidelobes effectively in the sub-bright region. Therefore, the number and characteristics of ship targets are distinct as shown in Figure 10b. As shown in Figure 10, these results show that the proposed algorithm improves the overall performance and accuracy of the radar system.

5. Conclusions

In this paper, we propose a novel range sidelobe suppression technique based on the non-grid multiple scattering points model. The improved MUSIC algorithm is utilized for time-delay super-resolution and accurate estimation of the scattering points' position offset information. By constructing the non-grid scattering signal model using precise non-grid offsets information, an iterative algorithm is employed to design optimal filters for each range unit adaptively. This approach enhances the detection performance of dense targets on non-grid significantly, while ensuring detection accuracy and performance. Since the sidelobes of strong points are easily confounded by noise and interference, traditional pulse compression methods may not be effective in suppressing the sidelobes. Through the adaptive pulse compression method, the proposed algorithm can suppress the sidelobe heavily and improve the anti-jamming ability in complex environments. In this way, it can accurately estimate the number and position of the targets and increase the sensitivity of the radar system. Therefore, the radar system detects more distant targets. In addition, traditional pulse compression methods are prone to false positives. However, the proposed algorithm reduces the probability of false alarm significantly and improves the accuracy and reliability of target detection by suppressing the sidelobes heavily. Therefore, this algorithm solves the challenge of detecting non-grid dense points effectively, and improves the overall detection performance and accuracy.

We achieve positive results based on this study while there is still room for improvement. In complex environments, such as the presence of strong interference or signal attenuation, the suppression effect of the algorithm may be affected, resulting in inaccurate positioning. We shall delve deeper into this algorithm, aspiring to attain greater breakthroughs in the times to come.

Author Contributions: Conceptualization, J.Z.; methodology, J.Z.; software, J.X.; validation, J.X.; investigation, Y.Z.; resources, J.C.; writing—original draft preparation, J.X.; writing—review and editing, J.Z.; supervision, J.Z. All authors have read and agreed to the published version of the manuscript.

Funding: This research was funded by National Natural Science Foundation (62171220).

Data Availability Statement: Not applicable

Conflicts of Interest: The authors declare no conflicts of interest.

References

1. Jiangbo, L.; Hongsheng, Y.; Dongbo, H.; Minh, N.D. Patch Match Filter: Efficient Edge-Aware Filtering Meets Randomized Search for Fast Correspondence Field Estimation. In Proceedings of the 2013 IEEE Conference on Computer Vision and Pattern Recognition, Portland, OR, USA, 23–28 June 2013; pp. 1854–1861.
2. Gerlach, K.; Blunt, S.D.; Picciolo, M.L. Robust Adaptive Matched Filtering Using the FRACTA Algorithm. *IEEE Trans. Aerosp. Electron. Syst.* **2004**, *40*, 929–945.
3. Li, K.; Yuan, L. The FIR Window Function Design Based on Evolutionary Algorithm. In Proceedings of the 2011 International Conference on Mechatronic Science, Electric Engineering and Computer (MEC), Jilin, China,19–22 August 2011; pp. 1797–1800.
4. Wu, X.; Liu, K.; Luo, M.; Shen, Q. LMMSE Channel Estimation Algorithm Based on Delay Time-Domain Windowing in AF Cooperative Systems. In Proceedings of the 2011 6th International ICST Conference on Communications and Networking in China (CHINACOM), Harbin, China, 17–19 August 2011; pp. 760–764.
5. Blinchikoff, H.J. Range Sidelobe Reduction for the Quadriphase Codes. *IEEE Trans. Aerosp. Electron. Syst.* **1996**, *32*, 668–675.
6. Fang, L.; Dong, D.; Boroyevich, D.; Mattavelli, P.; Wang, S. Improving High-Frequency Performance of an Input Common Mode EMI Filter Using an Impedance-Mismatching Filter. *IEEE Trans. Power Electron.* **2014**, *29*, 5111–5115.

7. Rao, M.N. Design of Mismatched Filters for Long Binary Codes. In Proceedings of the 2008 IEEE Radar Conference, IEEE, Rome, Italy, 26–30 May 2008; pp. 1–6.
8. Bose, R. Lean CLEAN: Deconvolution Algorithm for Radar Imaging of Contiguous Targets. *IEEE Trans. Aerosp. Electron. Syst.* **2011**, *47*, 2190–2199.
9. Zrnic, B.; Zejak, A.; Petrovic, A.; Simic, I. Range Sidelobe Suppression for Pulse Compression Radars Utilizing Modified RLS Algorithm. In Proceedings of the 1998 IEEE International Symposium on Spread Spectrum Techniques and Applications, Sun City, South Africa, 2–4 September 1998; pp. 1008–1011.
10. Yanming, L. Study on the Technology of Quadric Surface Extracting Base on Least Square Method. In Proceedings of the 2011 Second International Conference on Mechanic Automation and Control Engineering, Hohhot, China, 15–17 July 2011; pp. 5328–5331.
11. Jin, E.S.; Liu, L.L.; Bo, Z.Q.; Klimek, A. Parameter Identification of the Transformer Winding Based on Least-Squares Method. In Proceedings of the 2008 IEEE Power and Energy Society General Meeting-Conversion and Delivery of Electrical Energy in the 21st Century, Pittsburgh, PA, USA, 20–24 July 2008; pp. 1–6.
12. Blunt, S.D.; Gerlach, K. Adaptive Pulse Compression. In Proceedings of the 2004 IEEE International Radar Conference, Philadelphia, PA, USA, 18–21 December 2004; pp. 271–276.
13. Blunt, S.D.; Gerlach, K. Adaptive Pulse Compression via MMSE Estimation. *IEEE Trans. Aerosp. Electron. Syst.* **2006**, *42*, 572–584.
14. Blunt, S.D.; Gerlach, K. A Novel Pulse Compression Scheme Based on Minimum Mean-Square Error Reiteration. In Proceedings of the 2003 Proceedings of the International Conference on Radar, Adelaide, SA, Australia, 3–5 September 2003; pp. 349–353.
15. Blunt, S.D.; Smith, K.J.; Gerlach, K. Doppler-Compensated Adaptive Pulse Compression. In Proceedings of the 2006 IEEE Conference on Radar, Verona, NY, USA, 24–27 April 2006; pp. 1–6.
16. Gerlach, K.; Blunt, S.D. Radar Pulse Compression Repair. *IEEE Trans. Aerosp. Electron. Syst.* **2007**, *43*, 1188–1195.
17. Blunt, S.D.; Higgins, T. Achieving Real-Time Efficiency for Adaptive Radar Pulse Compression. In Proceedings of the 2007 IEEE Radar Conference, Waltham, MA, USA, 17–20 April 2007; pp. 116–121.
18. Blunt, S.D.; Higgins, T. Dimensionality Reduction Techniques for Efficient Adaptive Pulse Compression. *IEEE Trans. Aerosp. Electron. Syst.* **2010**, *46*, 349–362.
19. Henke, D.; Mccormick, P.; Blunt, S.D.; Higgins, T. Practical Aspects of Optimal Mismatch Filtering and Adaptive Pulse Compression for FM Waveforms. In Proceedings of the 2015 IEEE Radar Conference, Arlington, VA, USA, 10–15 May 2015; pp. 1149–1155.
20. Henke, D. Robust Optimal and Adaptive Pulse Compression for FM Waveforms; University of Kansas: Kansas, MS, USA, 2015.
21. VanTrees, H.L. *Optimum Array Processing Part IV of Detection, Estimation and Modulation Theory*; John Wiley and Sons Inc.: New York, NY, USA, 2002; pp. 513–518.
22. Geng, Z.; Deng, H.; Himed, B. Adaptive Radar Beamforming for Interference Mitigation in Radar Wireless Spectrum Sharing. *IEEE Signal Process. Lett.* **2015**, *22*, 484–488.
23. Su, H.; Liu, H.; Shui, P.; Bao, Z. Adaptive Beamforming for Nonstationary HF Interference Cancellation in Skywave Over-the-Horizon Radar. *IEEE Trans. Aerosp. Electron. Syst.* **2013**, *49*, 312–324.
24. Blunt, S.D.; Gerlach, K. Adaptive Pulse Compression Repair Processing. In Proceedings of the 2005 IEEE International Radar Conference, Arlington, VA, USA, 29 July 2005; pp. 519–523.
25. Shackelford, A.K.; De Graaf, J.; Talapatra, S.; Blunt, S.D.; Gerlach, K. Adaptive Pulse Compression: Preliminary Experimental Measurements. In Proceedings of the 2007 IEEE Radar Conference, Waltham, MA, USA, 17–20 April 2007; pp. 234–237.
26. Baghel, V.; Panda, A.; Panda, G. An Efficient Hybrid Adaptive Pulse Compression Approach to Radar Detection. In Proceedings of the 2013 International Conference on Signal Processing and Communication, Noida, India, 12–14 December 2013; pp. 335–339.
27. Qianrong, L.; Xiji, W.; Zhicheng, W.; Xiaochao, M.; Na, Y. Robust Adaptive Pulse Compression Under Encode-Decoder Network for Synthetic Aperture Radar. In Proceedings of the 2021 Asia-Pacific Conference on Synthetic Aperture Radar (APSAR), Bali, Indonesia, 1–5 November 2021; pp. 1–5.
28. Qianrong, L.; Wenming, T.; Qingqing, L.; Bingqi, Z.; Ke, D.; Xiangzhen, Y. Robust Adaptive Pulse Compression for Synthetic Aperture Radar. In Proceedings of the 2021 China International SAR Symposium (CISS), Shanghai, China, 3–5 November 2021; pp. 1–6.
29. Higgins, T.; Blunt, S.D.; Gerlach, K. Gain-Constrained Adaptive Pulse Compression via An MVDR Framework. In Proceedings of the 2009 IEEE Radar Conference, Pasadena, CA, USA, 12–16 October 2009; pp. 1–6.
30. Akdemir, Ş.B.; Candan, Ç. Study of Angle of Arrival Estimation Performance of MVDR and Capon Methods under Intermittent Interference. In Proceedings of the 2018 Signal Processing and Communications Applications Conference (SIU), Izmir, Turkey, 2–5 May 2018; pp. 1–4.